A Modeling Study Evaluating the Thermal-Hydrological Conditions in and Near Waste Emplacement Tunnels at Yucca Mountain

J.T. Birkholzer[1], N. Halecky[1+3], S. W. Webb[2], P. F. Peterson[3], and G.S. Bodvarsson[1]*

[1]*Lawrence Berkeley National Laboratory, Berkeley, CA*
[2]*Sandia National Laboratories, Albuquerque, NM*
[3]*University of California at Berkeley, Berkeley, CA*

*Corresponding Author: J.T. Birkholzer
          Tel. 1 510 486 7134
          Fax 1 510 486 5686
          Email: jtbirkholzer@lbl.gov

Total Number of Figures: 13
Total Number of Tables: 1
Total Number of Pages: 44

ABSTRACT

In heated tunnels such as those designated for emplacement of radioactive waste at the proposed geologic repository at Yucca Mountain, temperature gradients cause natural convection processes that may significantly influence the moisture conditions in the tunnels and in the surrounding fractured rock. Large-scale convection cells in the heated tunnels would provide an effective mechanism for turbulent mixing and axial transport of vapor generated from evaporation of pore water in the nearby formation. As a result, vapor would be transported from the elevated-temperature sections of the tunnels into cool end sections (where no waste is emplaced), would condense there, and subsequently drain into underlying rock units. To study these processes, we have developed a new simulation method that couples existing tools for simulating thermal-hydrological (TH) conditions in the fractured formation with a module that approximates turbulent natural convection in heated emplacement drifts. The new method simultaneously handles (1) the flow and energy transport processes in the fractured rock, (2) the flow and energy transport processes in the cavity, and (3) the heat and mass exchange at the rock-cavity interface. An application is presented studying the future TH conditions within and near a representative waste emplacement tunnel at Yucca Mountain. Particular focus is on the potential for condensation along the emplacement section, a possible result of heat output differences between individual waste packages.

I.   INTRODUCTION

Extensive scientific investigations have been conducted at Yucca Mountain, Nevada, to explore whether the site is suitable for geologic disposal of radioactive waste (Bodvarsson et al., 1999). If constructed, the repository will be located in partially saturated fractured rock several hundred meters above the groundwater table, at a depth of about 300 m below the ground surface. In the current design, cylindrical waste canisters will be distributed along horizontal tunnels of 5.5 m diameter and several hundred meters in length. The heat produced by the radioactive waste will significantly change the thermal and hydrological environment at Yucca Mountain, affecting both the host rock and the conditions in the tunnels. Pore-water vaporization and subsequent condensation will lead to a large saturation and flux redistribution in the near-field fractured rock. Also, as vapor enters the emplacement tunnels (drifts), the vapor concentration near waste packages will increase. Understanding these changes—in both the natural system and the drifts—is essential for evaluating the future performance of the repository in terms of canister corrosion and radionuclide containment.

The thermally driven flow processes to be expected in the fractured rock at Yucca Mountain have been investigated in various modeling studies (e.g., Pruess et al., 1990a, 1990b; Buscheck et al., 2002; Haukwa et al., 2003; Birkholzer et al., 2004). Gas flow along emplacement drifts has usually been neglected in these models, either because individual drifts were not represented at all or were treated as closed systems without axial flow and transport components. As a result, the models predict that the majority of the vapor produced from boiling/evaporation of formation water would remain in the fractured rock. Simulations presented in this paper show that there may be considerable vapor transport from the fractured formation into the emplacement drifts. Recent computational-fluid-dynamics (CFD) simulations suggest that large-scale axial

convection cells would form within emplacement drifts (Webb and Itamura, 2004; Webb and Reed, 2004), which, combined with turbulent mixing due to natural convection flows induced by heat transport from the canisters to the drift walls, would provide an important transport mechanism that can move vapor away from the vapor-producing drift sections to the cold end of the drifts. To estimate the magnitude of vapor transport, the calculated dispersion coefficients were used as input to a semi-analytical model for one-dimensional heat and vapor transport along drifts (Webb and Reed, 2004). The analysis demonstrated the importance of convective mixing between vapor-rich (hot) and vapor-poor (cool) drift sections. However, while the in-drift processes were captured in detail, the presence of the fractured rock was approximated using precalculated boundary conditions, thus neglecting the important feedback between the in-drift and the fractured-rock TH conditions. An alternative methodology with a more sophisticated treatment of the near-drift formation was developed by Danko et al. (this issue), using an efficient iterative procedure to decouple the drift and rock-mass formulations.

In this paper, we describe and apply a new simulation method that simultaneously handles mass and heat transport in the fractured formation *and* in the emplacement drifts. The model concepts used for the partially saturated fractured rock are based on existing porous-medium models for Darcy-type flow and transport as described, for example, in Haukwa et al. (2003) and Birkholzer et al. (2004). In-drift natural convection and turbulent mixing is approximated as a binary diffusion process, with effective mass-dispersion coefficients estimated from supporting CFD analyses described in Webb and Itamura (2004) and Webb and Reed (2004). Mass and heat transfer between the formation and the drift are approximated by empirical boundary-layer correlations (Kuehn and Goldstein, 1976, 1978; Raithby and Hollands, 1985), based on a methodology developed in Webb and Reed (2004). We implemented the new drift natural

convection module into TOUGH2, a general-purpose simulator for coupled transport of multiphase, multicomponent fluid mixtures in porous and fractured media (Pruess et al., 1999). The governing equations for the integrated drift and rock-mass model are solved in a fully coupled, noniterative manner, ensuring consistency between the thermal-hydrological conditions in the fractured rock and those in the open drift.

In previous analyses (Birkholzer et al., 2006a, 2006b), the above-described TOUGH2 simulation method was applied to better understand how natural convection in Yucca Mountain drifts would affect the near-drift TH processes, particularly with respect to the saturation changes and flux perturbations in the fractured rock. In this paper, we conduct similar analyses, but focus on the potential for in-drift condensation as triggered by the considerable heat-output differences between individual waste packages. Our three-dimensional model domain comprises one representative drift and the surrounding fractured rock, with two 40 m long drift sections discretized in detail such that the heat output of individual waste packages can be simulated. While conclusions are drawn with respect to the potential impact of our findings on repository performance, it is important to realize that our modeling approach (see Section III below) includes a number of limiting assumptions and geometrical simplifications that are valid for a comparative evaluation, but should not be interpreted as a realistic quantitative representation of the system behavior at Yucca Mountain.

II. BASIC TH PROCESSES

The current DOE design for the geologic repository at Yucca Mountain envisions emplacement of waste canisters in a large number of parallel drifts spaced 81 m apart. Typically, these drifts have an emplacement section about 600 m long followed by unheated end sections (turnout

sections), that can be as long as 100 m or more. In contrast to the access drifts and shafts, which will be backfilled with crushed tuff material, the emplacement drifts, including their end sections, may remain open. The cylindrical waste canisters, about 5 m long and between 1.75 m and 2.11 m in diameter, are distributed horizontally along the drifts, with an axial distance of 0.1 m between them. A drip shield covers the waste packages and protects them from rock fall and water seepage. Current design estimates for waste package loading at Yucca Mountain assume an initial heat load for the radioactive waste of 1.45 kW per meter drift length, which represents the average heat load for different waste packages (BSC, 2003a). The initial load decreases with time as a result of radioactive decay.

In the open drifts at Yucca Mountain, the heat emanating from the waste packages will be effectively transferred to the drift walls, mostly via thermal radiation. At early stages after emplacement, temperatures in the partially saturated formation near the drifts will heat up to above-boiling conditions. As a result, the initially mostly stagnant pore water in the rock matrix will become mobile through boiling (see Figure 1a). This will create a pressure increase, which will drive the vapor into the highly permeable fractures that are pervasive in the repository rock layers. The vapor will then move away from the boiling region through the fracture network, both into more distant rock regions (where the vapor will condense and enhance liquid fluxes) and into the drifts. (It can be assumed that the gas pressure within the drifts will remain at ambient atmospheric conditions, because any pressure increase would vanish in the axial direction, owing to the good communication of the drift with the main access tunnels and the large rock volumes.) Simultaneously, vapor concentrations will increase, causing diffusive transport away from the heated regions. At later times, when temperatures decrease below boiling, the rock mass near the drifts will gradually rewet, allowing for evaporation of pore water from the drift walls (Figure 1b). For drifts with average temperature conditions, rewetting will

occur roughly a few hundred years after boiling has ceased (Birkholzer et al., 2004), a time period in which natural convection processes within the drifts are still effective.

Vapor entering the emplacement drifts from the fractured porous rock is subject to effective radial and axial mixing transport, as a result of turbulent natural convection processes occurring in the open gas space. Axial mixing can reduce the overall moisture content in heated drift sections because of the presence of the unheated drift ends (turnouts). Principles of thermodynamics suggest that the maximum amount of vapor that can be present in air decreases with declining temperature. Thus, the warm vapor-rich gases moving from heated drift sections toward the drift turnouts—caused by turbulent mixing and natural convection processes—will be depleted of most of their vapor content through condensation on cooler rock surfaces. (Note that the condensate will drain away from the repository into underlying rock units.) At the same time, vapor-poor gas will recirculate towards the emplacement sections of the drifts, thereby reducing the moisture content and relative humidity in these areas (Birkholzer et al., 2006a, 2006b). This effect, in turn, will generate a concentration gradient between the fractured rock and the in-drift environment, causing diffusive vapor transport from the formation into the drift, in addition to the convective vapor transport caused by the formation pressure increase during boiling.

While most of the condensation is expected to occur in the unheated drift turnouts, temperature variation between individual waste packages may also cause local condensation along the heated drift section (Figure 1b). The potential for and the magnitude of local condensation depend on the average moisture content in the heated drifts in conjunction with local temperature and relative humidity variability.

III.   MODELING APPROACH

III.A   Modeling Framework for Fractured Rock Mass

As mentioned before, the modeling framework for simulating the TH conditions in the near-field fractured rock is adopted from existing TH models for Yucca Mountain (e.g., Haukwa et al., 2003; Birkholzer et al., 2004). The relevant TH processes in the heated rock mass are convective and diffusive movement of gaseous and liquid phases of water and air (under pressure, viscous, capillary, and gravity forces); transport of latent and sensible heat; phase transition between liquid and vapor; and vapor-pressure lowering (Pruess et al., 1999). Fluid flow is described with a multiphase extension of Darcy's law. Heat transfer occurs by conduction, convection, and phase change. The fractured rock is described using a dual permeability concept, assuming two separate but interacting continua that superpose with each other in space. One continuum describes flow and transport in the highly-permeable fracture network (continuum permeability on the order of 10^{-13} m^2), the other describes flow and transport in the low-permeability rock matrix (average permeability on the order of 10^{-18} m^2), with local exchange (e.g., energy transfer, imbibition, matrix diffusion) between the two continua as a result of differences in TH conditions. Thus, disequilibrium conditions between fractures and matrix and the corresponding mass and heat transfer can be efficiently modeled without explicitly accounting for all individual fractures and matrix blocks. Birkholzer et al. (2006b) provide more details.

III.B   Modeling Framework for Emplacement Drifts

In principle, the mass and heat transport processes occurring in an open drift could be modeled with a CFD simulator that would solve the mass, momentum, and energy conservation equations, including their turbulent contributions (e.g., Webb and Itamura, 2004; Webb and Reed, 2004). However, solving the turbulent velocity fields expected in heated drift sections would require

fine spatial and temporal resolution. Not only would this result in highly time-consuming simulation runs, but would also necessitate complex coupling approaches, because of the large discretization disparities between the drift and the fractured rock.

For the purpose of this study, we follow the methodology described in Webb and Itamura (2004), and assume that the axial transport of vapor and air can be approximated as a binary diffusion process of the air-vapor mixture, using effective mass dispersion coefficients calculated from complementary CFD flow-field simulations. By approximating natural convection as a binary diffusion process, then the vapor mass transport that would occur due to in-drift heat and fluid flow processes can, in principle, be reproduced with the standard methodologies applied for Darcy-type flow and transport (such as those implemented in TOUGH2), with the drift represented as a specific solution subdomain that requires certain code modifications and parameter specifications. A new drift simulation version of TOUGH2 was developed that can solve simultaneously for heat and fluid flow within the drift and in the surrounding rock mass. A brief review of the most important code modifications is given below; more details are given in Birkholzer et al. (2006b):

- Users may define natural-convection subdomains in which binary diffusion is calculated using predefined values for the effective mass dispersion coefficients. For simplification, the coefficients are assumed to be identical in the axial and radial directions. Drift elements representing such subdomains are assigned the thermophysical properties (density, thermal conductivity, heat capacity) of vapor-air mixtures at prevailing temperatures and pressures.

- The heat and mass transfer between the gas flow in the natural-convection subdomain and the near-drift fractured rock is calculated from empirical boundary-layer correlations given in the literature (Kuehn and Goldstein, 1976 and 1978; Raithby and Hollands, 1985). This transfer

is affected by the presence of a surficial fluid boundary layer, where the motion of fluid is retarded compared to the free stream velocity. The correlations used in this study were derived for free convection in the annular space between horizontal eccentric cylinders, which roughly represents the geometry of an open drift with a drip shield/waste package assembly. See details in Webb and Reed (2004) and Birkholzer et al. (2006b).

- The new TOUGH2 version allows for the definition of thermal-radiation-only connections, where all other heat- and mass-transport processes are eliminated. Users can define direct radiative connections between emitting (waste packages) and receiving surfaces (drift wall, invert) across open gas spaces that are finely discretized to allow for in-drift mass and heat transfer. Similar to the standard TOUGH2, thermal radiation is described with the Stefan-Boltzmann equation (Pruess et al., 1999). A new preprocessing code was developed that calculates three-dimensional view factors for a detailed representation of radial and axial surface-to-surface radiation.

III.C   Model Setup

Three-dimensional simulation runs were performed for a simplified geometrical representation of an emplacement drift located in one of the southern panels of the proposed repository layout (Figure 2). The model domain comprises the entire unsaturated zone, having the ground surface as the upper model boundary and the groundwater table as the lower model boundary. In axial drift direction (y-direction), symmetry is assumed, which allows for reducing the model to half of the drift length. Thus, the simulated drift comprises half of the typical emplacement section length (300 m), followed by an 80-m unheated section away from the symmetry axis. The total length of the model domain in y-direction is 520 m, which includes the 380 m long drift plus a 130 m extent of fractured rock beyond the end of the drift. Symmetry assumptions can also be used to reduce the model domain in the x-direction, perpendicular to the drift axis. The current

repository design of parallel drifts can be represented as a series of symmetrical, identical half-drift domains with vertical no-flow boundaries between them. Thus, the numerical mesh can be limited to a lateral width of 40.5 m, extending from the drift center to the midpoint between drifts.

The three-dimensional grid used in the simulations comprises about 14,000 finite volumes with about 50,000 connections. Figure 2 shows the grid in a vertical cross section orthogonal to the drift axis (x-axis). Focusing on in-drift and near-drift conditions, it is important to represent the drift and its vicinity with a refined discretization. Simplifications are necessary, on the other hand, to ensure that the simulation effort is not excessive. For example, the waste package, the drip shield, and the small air space between them are treated in our study as a lumped entity in the simulation runs with equivalent thermal properties (based on averaging the respective thermal properties of the waste package, drip shield, and air). Thus, the flow and transport processes occurring under the drip shield and in the gap between waste packages are neglected in this study.

As shown in Figure 3, the numerical grid comprises various vertical slices of varying thickness along the drift axis (y-axis), ranging from less than 5 m to about 50 m. Similar to BSC (2005), there are two finely gridded segments along the emplacement section of the drift—one near the drift center, the other at the end of the emplacement section—where the thickness of the vertical slices corresponds to the axial length of individual waste packages. Only in these segments is the strong heat output variability between waste packages taken into account; i.e., the potential for local condensation can be evaluated. Waste packages are arranged in sequence according to an idealized design option described in BSC (2003a), with a cool waste package such as the

"5 HLW" situated next to hotter waste packages such as the "21 PWR AP (Hot)" or the "44 BWR AP" (Figure 3). For grid efficiency purposes, all other emplacement regions have the average decay heat imposed as a uniform axial line load.

The thermal load of all waste packages is time-dependent (Figure 4), exponentially decaying from an initial value that ranges between 0.2 kW (for the "5 HLW LONG") and 2.3 kW per meter drift length (for the "21 PWR AP (Hot)"). For comparison: the initial value for an average thermal line load (TLL) is 1.45 kW/m. Note that a considerable amount of the decay heat is removed by forced drift ventilation during the first 50 years after emplacement (preclosure period). Similar to previous studies (e.g., Haukwa et al., 2003; Birkholzer et al., 2004), forced drift ventilation is not explicitly modeled in our simulations. Rather, the heat losses by forced drift ventilation are incorporated by reducing the effective heat output in the simulation to about 14% of its original value, based on design estimates provided in BSC (2004).

As pointed out before, natural convection is treated as a binary diffusion process in this study, with effective diffusion coefficients derived from CFD studies. There is, however, considerable uncertainty as to the magnitude of these coefficients. Two vastly differing sets of dispersion values were derived in Webb and Itamura (2004), representing first-order estimates for the possible range of natural convection conditions in Yucca Mountain drifts (see Table 1). To account for this uncertainty, we run two main simulation cases, one with strong convective mixing (Case 1), the second with moderate convective mixing (Case 2). All drift elements representing the open enclosure, in both emplacement section and unheated end section of the drift, are assigned the effective dispersion coefficients as uniform values. Other material

properties and the model boundary conditions are described elsewhere (e.g., Birkholzer et al., 2006b) and shall not be repeated here.

IV. MODEL APPLICATION AND RESULTS

Our model simulations cover the first 4,000 years after emplacement of radioactive waste into a representative drift. Being most interested in the effects of natural convection, we focus on the postclosure period, which follows the forced-ventilation preclosure period of 50 years. Our aim in this paper is to evaluate the potential for local condensation in the vicinity of comparably cool waste packages. Condensation can only occur when the local temperature drops below the boiling point of water. Previous experience with similar models has shown that this is to be expected between 600 and 1,000 years after waste emplacement (Birkholzer et al., 2006a, 2006b). A simulation period of 4,000 years ensures that a significant time period with sub-boiling conditions is covered.

In light of the primary interest of the study, the main focus in the discussion of model results is on the TH conditions within the drifts, which are described in Sections IV.B and IV.C. However, to provide the necessary context for the discussion of in-drift processes, we start Section IV.A below with a brief review of the main TH model results for the near-field fractured rock mass. More details on the TH conditions in the near-field formation can be found in two previous papers (Birkholzer et al., 2006a, 2006b).

IV.A   TH Processes in Near-Field Fractured Rock

We present the TH processes in the near-field fractured rock using Case 1 as an example, which features strong convective mixing along the drift, and select the conditions in a vertical cross

section along the drift at 500 years after emplacement, representative of the expected situation towards the end of the boiling period at Yucca Mountain. Figure 5a depicts temperature and liquid saturation contours for the fracture continuum and the drift, while Figure 5b plots vapor concentration (derived as the mass fraction of vapor in the gas phase) and liquid saturation contours in the matrix continuum and in the drift. For better visualization, we focus on the drift vicinity (with vertical extension from -40 m $\leq$ z $\leq$ 40 m), and zoom in on the two finely gridded drift sections with individual waste packages, one close to the center of the drift and one towards the drift end. Note that in this figure, and all other profile plots to follow, the distance along the drift is measured from the center of the heated section of the drift, the symmetry boundary of the half-drift model. The heated section of the drift ends at about 300 m, followed by the 80 m long unheated end section.

Before evaluating heat-related flow and transport processes, we should briefly discuss the ambient (initial) situation in the partially saturated repository units at Yucca Mountain, where natural infiltration is very small on the order of a few millimeter per year. As a result of the small infiltration into the unsaturated zone, the fractures are essentially drained of water and nonconductive, with the saturation value close to residual. The matrix pores, on the other hand, hold a significant amount of water owing to strong capillary forces, with saturation values of the order of 0.85. However, despite the relatively large saturation, the water in the matrix is almost stagnant at ambient because of the very low matrix permeability. Prior to heating, the temperature is about 25°C at the repository depth, and the gas pressure is close to atmospheric pressure at the elevation of Yucca Mountain (about 89000 Pa). The ambient vapor concentration in the gas phase is very small, corresponding to a relative humidity of 100% at 25°C.

Both the matrix and fracture saturation contours show that a large volume of rock has desaturated in the vicinity of the heated section of the drift, with the region of reduced liquid saturation extending several meters into the formation. Because significant amounts of pore water have boiled off, the simulated vapor concentration in the gas phase has increased significantly in the heated rock region, with maximum values above 0.6 a few meters away from the drift (initial vapor concentration at ambient conditions is close to zero). Part of the vapor moves effectively within the highly permeable fractures out into the distant rock mass. As a result, elevated vapor concentrations of 0.3 and more can be seen at distances of 30 m above and below the heated drift.

Notice the pronounced saturation buildup near the unheated end section of the drift in both Figures 5a and 5b, indicating that a significant amount of the vapor produced in the rock mass enters the drift, migrates in axial direction (as a result of turbulent mixing and circulating gas flows from natural convection), and eventually condenses on the cooler drift wall surfaces (Figure 5a). According to the model predictions, most of the condensate drains towards the drift bottom through the invert and downward into the fracture continuum. As a result, fracture saturation increases strongly below the drift, and significant gravity-driven liquid fluxes occur, driving water away into the underlying formations. A small fraction of the condensate imbibes from the drift walls into the matrix pores as a result of capillary forces. The impact of imbibition can be seen in the elevated matrix saturations both above and below the drift end (Figure 5b).

While vapor-rich gas is driven from the heated drift section towards the unheated drift turnout, vapor-poor gas moves back, thereby reducing the in-drift vapor concentration near the heat-producing waste packages. This effect, present along the entire length of the emplacement

section, causes a steep vapor concentration gradient between the fractured rock mass and the drift. For example, Figure 5b shows that the simulated maximum vapor concentration in the drift is between 0.2 and 0.3, which compares to a maximum value of more than 0.6 in the rock. As a result of this concentration difference, vapor migrates from the heated rock mass into the drift not just by pressure-driven convective flow, but also by diffusion.

Whereas the heat-induced moisture redistribution processes are in general similar, Case 2 differs from Case 1 in that the convective mixing between vapor-rich and vapor-poor regions of the drift is less effective. As a result, in Case 2, more vapor remains in the heated rock mass where it is produced, and less vapor migrates from the heated drift section towards the cooler drift turnout. Figure 6 compares vapor-flux profiles from the formation into the drift at 500 years after emplacement between Cases 1 and 2. The vapor-flux profiles are given as relative values, divided by the total liquid flux arriving over the footprint of the heated drift section from ambient percolation. A relative vapor flux of one, for example, means that the vapor mass migrating from the formation into the drift is identical to the liquid mass arriving via percolation. The figure exemplifies the magnitude of formation-to-drift vapor transport, particularly in Case 1, where natural convection is strong: over most of the heated drift section, the amount of vapor transferred into the drift is between three and four times higher than the water arrival from natural percolation, suggesting that the vapor source is mostly resident pore water. Less vapor transfer is observed in Case 2, with relative vapor fluxes around two. Both cases exhibit almost no vapor transfer in the unheated end section of the drift, where temperatures drop significantly over a relatively short distance.

IV.B   In-Drift TH Conditions

First, let us examine the simulated temperature response in the drift as a function of time. Figure 7 shows temperature profiles along the open drift close to the crown, for Case 1 with strong convective mixing and Case 2 with moderate convective mixing. In both cases, the emplacement section of the drift heats up strongly to about 140°C at 100 years after waste emplacement. The temperature trend reverses at later stages, when the reduced heat output of the radioactive waste (see Figure 4) results in a gradual temperature decrease. At 500 years, for example, the in-drift temperatures have reduced to a few degrees centigrade above boiling along most of the heated section. As discussed in the previous section, the heating of the rock mass causes boiling of pore water in the adjacent rock mass during this early emplacement period, combined with significant vapor transport into the heated drift. At later times, between 500 and 1,000 years, the heated section of the drift drops completely below the boiling temperature, creating the potential for water vapor to condense on the drift walls near the cooler waste packages. All temperature profiles, even at 4,000 years after emplacement, remain elevated from ambient, and exhibit moderate to strong temperature differences between the heated drift section and the unheated end (indicating that natural convection processes will still be relevant even at these later times).

We observe that the varying heat output of the individual waste packages causes considerable temperature differences between neighboring drift crown segments. At 100 years, these differences are larger than 5°C near the "5 HLW Long" waste packages, which have the smallest thermal load, and a little less than 5°C near the "5 HLW Short" waste packages, which have the second-smallest thermal load (see Figures 3 and 4). Even at 1,000 years, when the drift crown temperature has dropped below boiling, there exists a roughly 2°C difference between the "21 PWR AP (Hot)" and the "5 HLW Long" waste packages for both simulation cases. With this

temperature difference occurring over a short distance of 5 m, areas near the cool waste package might act as localized "cold traps" for water vapor to condense.

Overall, the temperature differences between Case 1 and Case 2 are rather subtle, indicating that the axial transport of sensible and latent heat with the gas flow in the drift is not overly important for the in-drift temperature distribution. The temperatures for the case with strong convective mixing are slightly lower in the heated section and slightly higher in the end section of the drift, a result of the more effective convective heat transport and the transport of latent heat in vapor in axial direction.

In Figure 8, we evaluate the predicted temporal evolution of vapor concentration (calculated as mass fraction of vapor in the gas phase) along the drifts for the two simulation cases. As mentioned before, Case 2 differs from Case 1 in that the convective mixing between the vapor-rich heated section and the vapor-poor end section of the drift is less effective. As a result, the amount of vapor in the emplacement section is much higher in Case 2 at all times, with maximum vapor concentrations of about 0.9 at 100 years. Note that these maximum concentrations occur in the drift center, and that values decrease significantly when approaching the end of the heated section. This suggests that convective mixing is not strong enough in Case 2 (i.e., that the turbulent circulation patterns are not large enough) to impact the entire emplacement drift; only those sections that are close to the unheated drift turnout are affected during these late time periods. In Case 1, on the other hand, the vapor concentrations are much smaller and more evenly distributed along the drift—the maximum vapor mass fraction is about 0.4 even at early times when significant amounts of vapor are produced from pore water boiling. Despite the large temperature differences between neighboring waste packages observed in

Figure 8, the gas in the open drift appears mixed well enough, in both cases, to allow for smooth vapor concentration profiles along the drift length.

Condensation of water vapor occurs when the gas reaches specific thermodynamic conditions, namely a pressure and temperature state, at which it is unable to contain any more water in the gas phase. The relative humidity, a ratio of the actual vapor pressure to the saturated vapor pressure, is an indicator of when these conditions for condensation exist. When the relative humidity of a gas is at 100%, any additional water vapor introduced must condense to liquid. To understand these effects on the in-drift environment in more detail, we compare the relative humidity of the gas at the drift crown along the length of the drift for both the strong and moderate convective mixing cases, as shown in Figure 9.

Independent of the simulation case, all relative humidity profiles exhibit relative humidities of 100% in the unheated end sections, indicating that condensation of water vapor will occur there. In the heated section, on the other hand, relative humidity is mostly lower than 100%, except for local peaks, and is generally smaller for Case 1 than for Case 2, a result of the more intense convective mixing between vapor-poor and vapor-rich drift sections. In fact, we observe that the relative humidity in Case 1 never reaches 100% over the entire heated length of the drift, making it impossible for local condensation to occur in this scenario. For Case 2, on the other hand, the relative humidity is near or reaches 100% at the cooler "5 HLW Long" and "5 HLW Short" waste packages at 1,000, 2,000, and 4,000 years after emplacement. Note that the local peaks in relative humidity are not a result of vapor concentration differences (which are minor according to Figure 9), but rather are mostly caused by the local temperature drops near the cooler waste packages.

We now analyze the expected magnitude and evolution of condensation in the drifts. We do this by plotting the amount of liquid water that leaves the drift at the bottom and drains out into the permeable fracture network. Since there is no seepage of liquid water from the formation into the drift because of considerable capillary forces, any water leaving the drift must be condensate that has entered in the form of vapor. We start by integrating the liquid fluxes draining out of the unheated end section of the drifts and plotting them as a function of time in Figure 10. Similar to Figure 6, the simulated fluxes are given as relative values, divided by the total flux arriving over the footprint of the heated drift section from ambient percolation.

We can observe that for Case 1, the maximum condensate flux leaving at the unheated drift end is about 10 times the percolation flux arriving over the drift footprint, occurring at about 75 years after emplacement. This large amount of condensate stems from vaporization of resident pore water in the surrounding rock. At later times, when temperatures have returned to below the boiling point, pore water evaporation is less significant. The flux reduces to relative values slightly less than one at 2,000 years after emplacement, and to about a quarter of the ambient percolation flux at 4,000 years. The sharp decline of the relative liquid flux around year 600 is caused by a stepwise increase in infiltration, which accounts for expected climate changes at Yucca Mountain in a simplified manner, based on analyses described in BSC (2003b). (Our work considers three long-term climate periods with constant infiltration: the present-day climate (up to 600 years from emplacement of waste), the monsoon climate (600–2,000 years), and the glacial transition climate (more than 2,000 years). During these periods, the imposed infiltration fluxes used in this work are 6, 16, and 25 mm/yr, respectively, representing average infiltration conditions.) In the moderate convective mixing case (Case 2), the relative liquid fluxes are much

smaller than what we observe in the strong convective mixing case. Initially around 5 times the ambient percolation flux, the condensate liquid flux is less than 10% of the ambient percolation at year 2,000, and less than 3% at 4,000 years. Because natural convection is less effective in Case 2, the amount of vapor transported along the drift is reduced compared to Case 1, and less condensate is thus deposited in the drift end section.

In Figure 11, we conduct a similar evaluation of condensate flux out of the drift bottom, but this time for specific segments along the emplacement section of the drift. As in Figure 10, fluxes are given relative to the percolation flux arriving over the footprint of the drift. Because of the vicinity to the waste packages, the existence of water in these segments is a concern to the performance of the repository. In Case 2, condensation occurs in the drift segments containing the "5 HLW Long" and "5 HLW Short" waste packages at both center and end drift locations. The maximum fluxes achieved are only 1–2% of the incoming percolation flux, indicating that the main fraction of the water vapor is transported to and condenses in the unheated drift ends. In Case 1, condensate is never observed at any time in any segment of the heated drift. This was already evident from Figure 9, since relative humidity never reaches 100%. Although the rate of vapor transfer from the formation into the drift is much higher than in Case 2, the strong convective mixing in Case 1 moves the vapor from the heated section to the drift end effectively enough to never allow for condensation.

Figure 11 indicates that local condensation observed in Case 2 is a transient process that differs between center and end sections of the drift. Condensation is first observed in the cool waste packages at the drift end (starting at 600 years), where the temperatures are generally lower and below-boiling conditions exist sooner than in the center. At later times, the drift center

temperatures also cool to below boiling, resulting in condensation there (starting at 900 years). The magnitude of local condensation reaches a maximum and then decreases with time. There may be two reasons for the transient decline in the condensate liquid fluxes: (1) with less heat emanating from the waste packages, the temperature difference between hot and cold waste package segments becomes smaller, (2) with the system slowly cooling (and less evaporation of pore water occurring), less moisture is transported from the formation into and along the drifts. After a few hundred years, condensation ceases in all cases except for the coolest "5 HLW Long" waste package in the drift center, where the condensate liquid flux goes through a minimum (at about 2,500 years), then increases slightly (possibly as a result of the increased infiltration in response to the assumed climate change), and eventually stabilizes at a relative value of less than 0.1%. That the drift-end waste packages behave differently from the drift-center waste packages may be related to the convective mixing in Case 2 not being strong enough to fully impact the entire emplacement drift. Note that in both locations, center and end, the magnitude of the fluxes from the "5 HLW Long" segments is larger than what is observed from the "5 HLW Short" segments. The difference here is not overall location of the waste packages along the drift, but rather the smaller decay heat output from the "5 HLW Long" waste package and the resulting lower temperature at the drift wall (see Figure 4).

Notice the initially steep increase in condensate liquid flux for the drift-end waste packages at about 600 years. Two significant changes are introduced into the simulation at this time, both of which contribute to trigger sudden condensation: (1) an increased infiltration flux representing the assumed climate change from present-day to monsoon conditions and (2) an instantaneous decrease in the vapor mass-dispersion coefficient for Case 2 as given in Table 1. An increase in infiltration provides more moisture in the near-drift formation, which would then increase the

amount of vapor transfer into the drift. A decrease in the mass-dispersion coefficients results in less effective axial exchange between vapor-rich and vapor-poor regions, causing an overall increase in moisture along the heated drift sections. Apparently, with these changes in the thermodynamic conditions, the moist air reaches saturation in the vicinity of the cooler waste packages, resulting in relatively sudden condensation.

IV.C   Impact of Partial Backfill in the Unheated End Section

This section investigates an alternative Yucca Mountain design option in which the unheated drift end sections (drift turnouts) are significantly shorter than the 80 m assumed in the previous simulations. It is possible that a majority of the drift turnouts will be backfilled with crushed tuff, to improve on drift stability. As a result, only a 20 m long unheated section would remain open at the end of the emplacement section in each drift, to be followed by a longer section filled with backfill material. The crushed tuff would be relatively small-grained; in other words, the backfill material would effectively block the natural-convection gas transport occurring in the open drift segments.

Below, we present simulation results with a TH model setup similar to that described in Sections IV.A and IV.B (referred to as base case), but with the drift turnout comprising a 20 m long open drift section followed by a 60 m long backfilled section. In the open drift section, natural convection is modeled using the same effective dispersion coefficients as in the base case. In the backfilled section, natural convection is not considered. It turns out that the effective length of the open, unheated end section has a significant impact on the simulated moisture redistribution and condensation results when strong convective mixing along the drift is assumed (i.e., using the effective dispersion coefficients of Case 1). Much less impact is seen in Case 2; therefore our sensitivity discussion focuses on the former case.

For the hot moist gases migrating down the drifts to be effectively depleted of their vapor, it is important that the unheated drift ends remain relatively cool. Our simulations suggest that a short end section heats up substantially by the strong convective transport of sensible and latent heat from the heated parts of the drift (Figure 12a). As a result of this temperature increase in the unheated ends, the saturation vapor pressure there increases and less condensation can occur. Compared to the base-case results for Case 1, this effect causes an overall much higher vapor concentration and relative humidity along the entire drift (Figures 12b and 12c). In fact, at 1,000 years and 2,000 years, the relative humidity in individual waste packages close to the drift end appears to be close to 100%, indicating that local condensation is possible there. In comparison, the base-case results for Case 1 exhibit relative humidity values well below 100% at all times (see Figure 9a). Figure 13 demonstrates that local condensation is indeed predicted for the alternative design in combination with strong convective mixing (Case 1). Both the "5 HLW Long" and the "5 HLW Short" segments close to the drift end exhibit relative condensation fluxes of up to 5% of the ambient percolation, so that overall, condensation occurs over considerable time periods of up to 3,000 years. In contrast, no local condensation is predicted for an 80 m long open end section, as discussed in Section IV.B.

V.   SUMMARY AND CONCLUSIONS

We have conducted a numerical study to evaluate how the vapor transport caused by natural convection in emplacement drifts at Yucca Mountain will affect the TH conditions (temperature, relative humidity, condensates) near waste packages. A new TOUGH2-based simulation method was developed that couples existing model approaches for predicting heat and mass transport in the rock mass with modules that approximate in-drift convection as a binary diffusion process.

Three-dimensional simulation runs were performed for a simplified geometrical representation of an emplacement drift, plus surrounding fractured rock, located in one of the southern panels of the repository. Two basic simulation cases were analyzed, representing different degrees of convective mixing in drifts, as determined from CFD studies reported in the literature.

Our simulation results demonstrate the importance of in-drift natural convection. Strong convective mixing:

- Causes considerable vapor transport from heated drift sections to unheated end sections
- Reduces relative humidity near waste packages
- Limits the potential for local condensation near cool waste packages.

These natural convection effects are expected to improve the performance of the repository, because the reduced relative humidity and reduced local condensation tends to form a more desirable waste package environment. However, there are strong differences between the two simulation cases representing strong versus moderate convective mixing. The latter case predicts local condensation to occur near cool waste packages over an extended time period. By contrast, local condensation does not occur in the former case, as strong convective mixing results in favorable relative humidity conditions. Considering these significant differences, we suggest that additional CFD modeling work and scaled laboratory experiments could better constrain the effects of natural convection and condensation in Yucca Mountain emplacement drifts.

Sensitivity studies demonstrate that the length of the unheated drift end section is also an important parameter determining the moisture and condensation conditions within emplacement drifts. It is shown that the benefits of natural convection may decrease significantly when the unheated end section becomes too short, in particular in the case of strong convective mixing.

Short end sections tend to heat up more easily from the mostly convective transport of heat along the drift, which means that the possible amount of vapor in the gas phase is higher before saturation is reached and condensation occurs. Thus, the gases that recirculate from the end sections towards the emplacement sections of drifts (as a result of convective mixing) contain more moisture than in the base case, causing the overall humidity levels to be higher along the heated drift segments.

While the results of our study have demonstrated the importance of natural convection in assessing the future TH conditions in Yucca Mountain drifts, it is important to consider that we have employed several limiting model assumptions. These assumptions are valid for a comparative evaluation of natural-convection sensitivity cases, but may not allow for a realistic quantitative representation of the future system behavior at Yucca Mountain. Among these are the approximation of in-drift flow patterns as a diffusive mixing process, the geometric simplification of the waste package and the drip shield as one lumped entity, and the relative coarseness of the in-drift discretization. Because of the latter assumption, the model does not predict patterns of relative humidity conditions below the resolution of one waste package.

REFERENCES

Birkholzer, J.T., S. Mukhopadhyay, and Y.W. Tsang, "Modeling Seepage into Heated Waste Emplacement Tunnels in Unsaturated Fractured Rock," *Vadose Zone Journal*, 3, 819–836, 2004.

Birkholzer, J.T., N. Halecky, S.W. Webb, P.F. Peterson, and G.S. Bodvarsson, "The Impact of Natural Convection on Near-Field TH Processes in the Fractured Rock at Yucca Mountain," Proceedings 2006 IHLRWM Conference, Las Vegas, May, 2006a.

Birkholzer, J.T., S.W. Webb, N. Halecky, P.F. Peterson, and G.S. Bodvarsson, "Evaluating the Moisture Conditions in the Fractured Rock at Yucca Mountain: The Impact of Natural Convection Processes in Heated Emplacement Drifts," Accepted for publication in *Vadose Zone Journal*, 2006b.

Bodvarsson, G.S., W. Boyle, R. Patterson, and D. Williams, Overview of Scientific Investigations at Yucca Mountain—The Potential Repository for High-Level Nuclear Waste, *Journal of Contaminant Hydrology*, 38(1–3), 3–24, 1999.

BSC, "Repository Design Project, IED Typical Waste Package Components Assembly," 800-IED-WIS0-00203-000-00B, Las Vegas, NE, Bechtel SAIC Company, 2003a.

BSC, "Analysis of Infiltration Uncertainty", ANL-NBS-HS-000027 REV 01, Las Vegas, NE, Bechtel SAIC Company, 2003b.

BSC, "Ventilation Model and Analysis Report," ANL-EBS-MD-000030 REV 04, Yucca Mountain Project Report, Bechtel SAIC Company, Las Vegas, Nevada, 2004.

BSC, "Multiscale Thermohydrologic Model," ANL-EBS-MD-000049 REV 03, Yucca Mountain Project Report, Bechtel SAIC Company, Las Vegas, Nevada, 2005.

Danko, G., J. Birkholzer, D. Bahrami, Coupled In-Rock and In-Drift Hydrothermal Model Study for Yucca Mountain, *Journal of Nuclear technology,* this issue.

Buscheck, T.A., N.D. Rosenberg, J. Gansemer, and Y. Sun, "Thermohydrologic Behavior at an Underground Nuclear Waste Repository," *Water Resources Research,* 38(3), 1–19, 2002.

Haukwa, C.B., Y.W. Tsang, Y.-S. Wu, and G.S. Bodvarsson, "Effect of Heterogeneity on the Potential for Liquid Seepage into Heated Emplacement Drifts of the Potential Repository," *Journal of Contaminant Hydrology*, 62–63, 509–527, 2003.

Kuehn, T.H., and R.J. Goldstein, "Correlating Equations for Natural Convection Heat Transfer in Between Horizontal Circular Cylinders," *International Journal of Heat and Mass Transfer*, 19, 1127–1134, 1976.

Kuehn, T.H., and R.J. Goldstein, "An Experimental Study of Natural Convection Heat Transfer in Concentric and Eccentric Horizontal Cylindrical Annuli," *Journal of Heat Transfer*, 100, 635–640, 1978.

Pruess, K., J.S.Y. Wang, and Y.W. Tsang, "On Thermohydrologic Conditions Near High-Level Nuclear Wastes Emplaced in Partially Saturated Fractured Tuff: 1. Simulation Studies with Explicit Consideration of Fracture Effects," *Water Resources Research,* 26, 1235-1248, 1990a.

Pruess, K., J.S.Y. Wang, and Y.W. Tsang, "On Thermohydrologic Conditions Near High-Level Nuclear Wastes Emplaced in Partially Saturated Fractured Tuff: 2. Effective Continuum Approximations," *Water Resources Research,* 26, 1249-1261, 1990b.

Pruess, K., C. Oldenburg, and G. Moridis, "TOUGH2 User's Guide, Version 2.0," LBNL-43134, Berkeley, California, 1999.

Raithby, G.D., and K.G.T. Hollands, "*Natural Convection,*" Chapter 6 of Handbook of Heat Transfer Fundamentals, McGraw-Hill Book Company, New York, Second Edition, 1985.

Webb, S.W., and M.T. Itamura, "Calculation of Post-Closure Natural Convection Heat and Mass Transfer in Yucca Mountain Drifts," Proceedings of 2004 ASME Heat Transfer/Fluids Engineering Summer Conference, Charlotte, NC, June 11–15, 2004.

Webb, S.W., and A. Reed, "In-Drift Natural Convection and Condensation," MDL-EBS-MD-000001 REV 00, Yucca Mountain Project Report, Bechtel SAIC Company, Las Vegas, Nevada, 2004.

List of Figures

Figure 12.   Results for sensitivity case with a 20 m long end section and strong convective mixing: (a) temperature, (b) vapor mass fraction, and (c) relative humidity. As in previous cases, the heated section of the drift ends at y = 300 m, but the 80 m long drift turnout has a 20 m long open section and a 60 m long backfilled section.

Figure 13.   Evolution of relative liquid flux from waste package segments for sensitivity case with a 20 m long end section and strong convective mixing. Liquid flux is normalized by dividing with ambient percolation flux integrated over the cross-sectional area of the drift. Local condensation occurs in the end section, not in the center section of the heated drift.

List of Tables

Table 1.   Mass dispersion coefficients (m^2/s) based on Webb and Itamura (2004)

(a)   Boiling Phase: Heated Drift Section Above Boiling Temperature

Boiling of Pore Water

Partially Saturated Rock Mass

Dryout Zone

Natural Convection

Drift Turnout

Vapor Transport

Water Drains Off

(b)   Sub-Boiling Phase: Heated Drift Section Below Boiling Temperature

Possible Condensation at Cool Waste Packages

Condensation

Vapor Transport

Drip Shield and Waste Packages

Vapor-Rich Gas   Vapor-Poor Gas
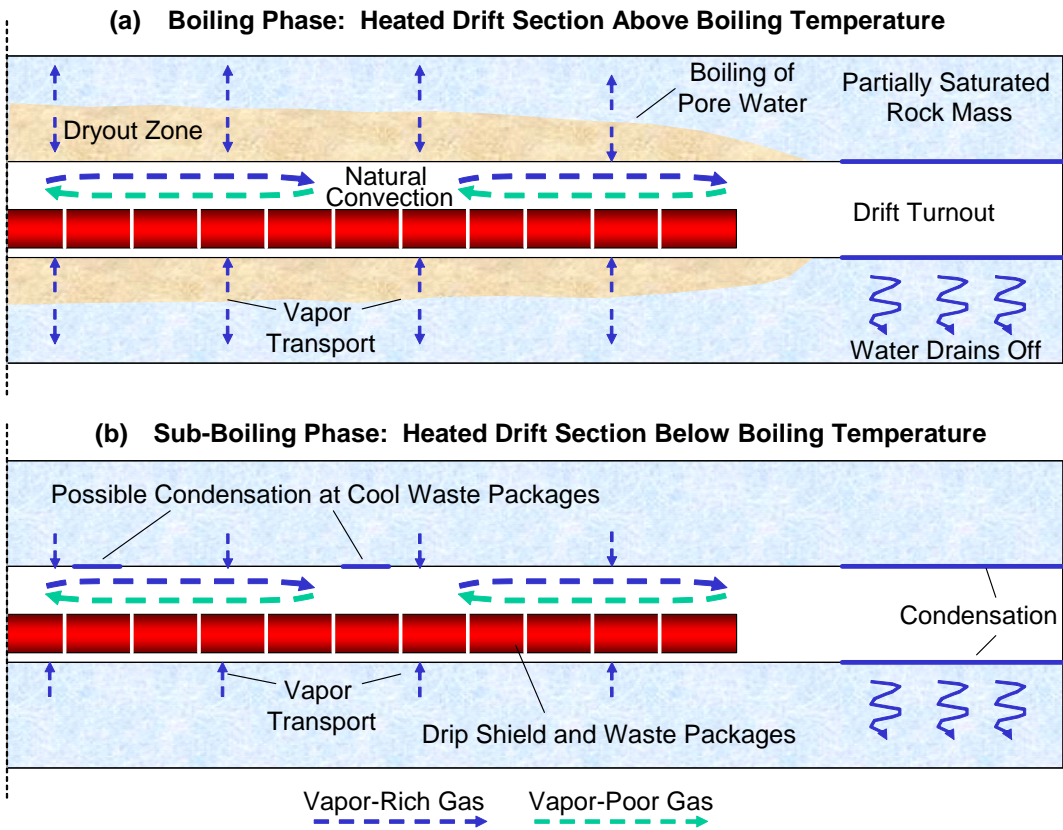
Figure 1.   Schematic of expected TH processes along an emplacement drift with individual waste packages (not to scale). The figure depicts part of a drift with emplacement and turnout sections (modified from Webb and Reed, 2004).
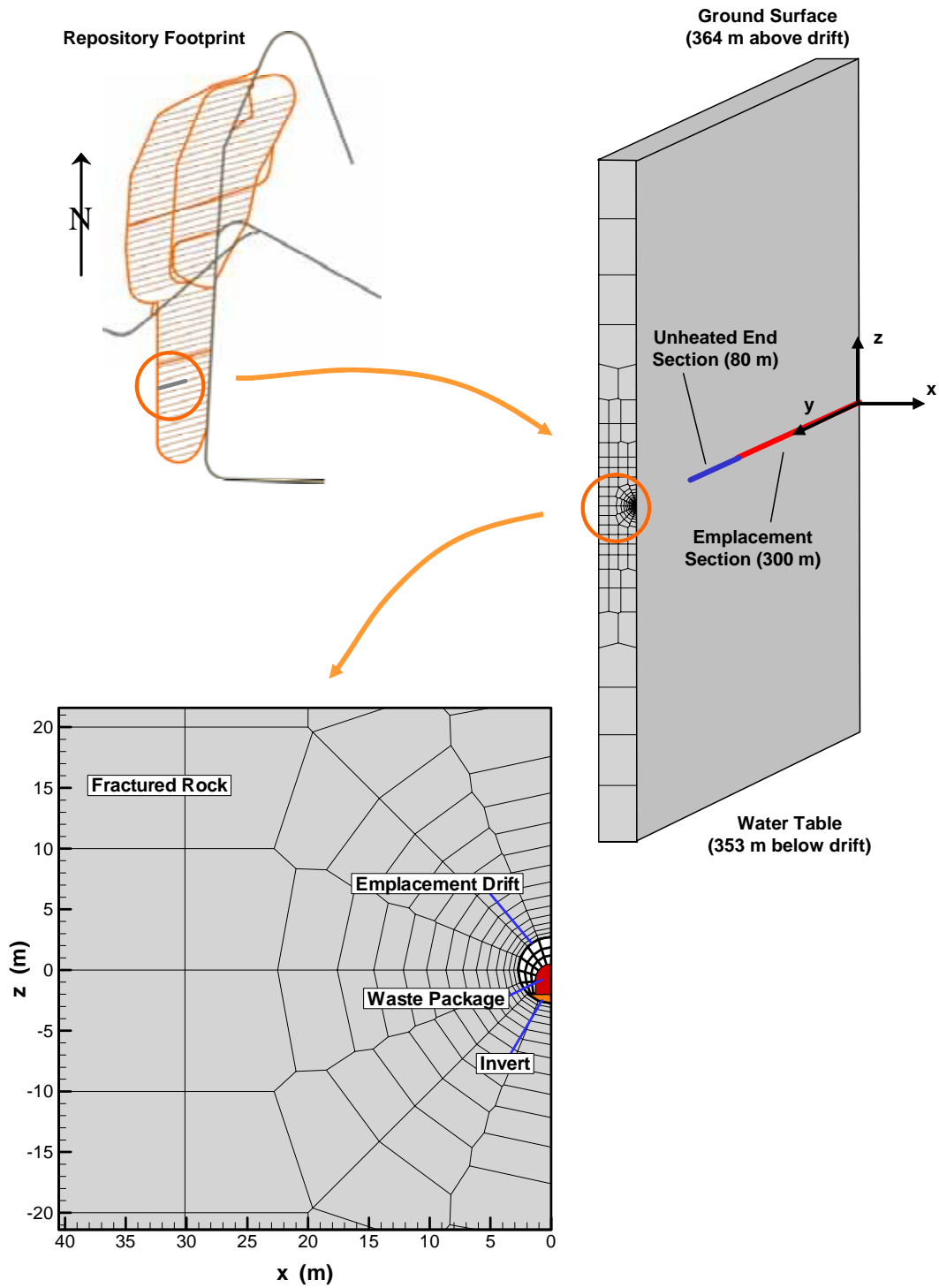
Figure 2. *Schematic showing the geometry of the three-dimensional model domain (not to scale). Close-up view shows discretization of drift and drift vicinity.*
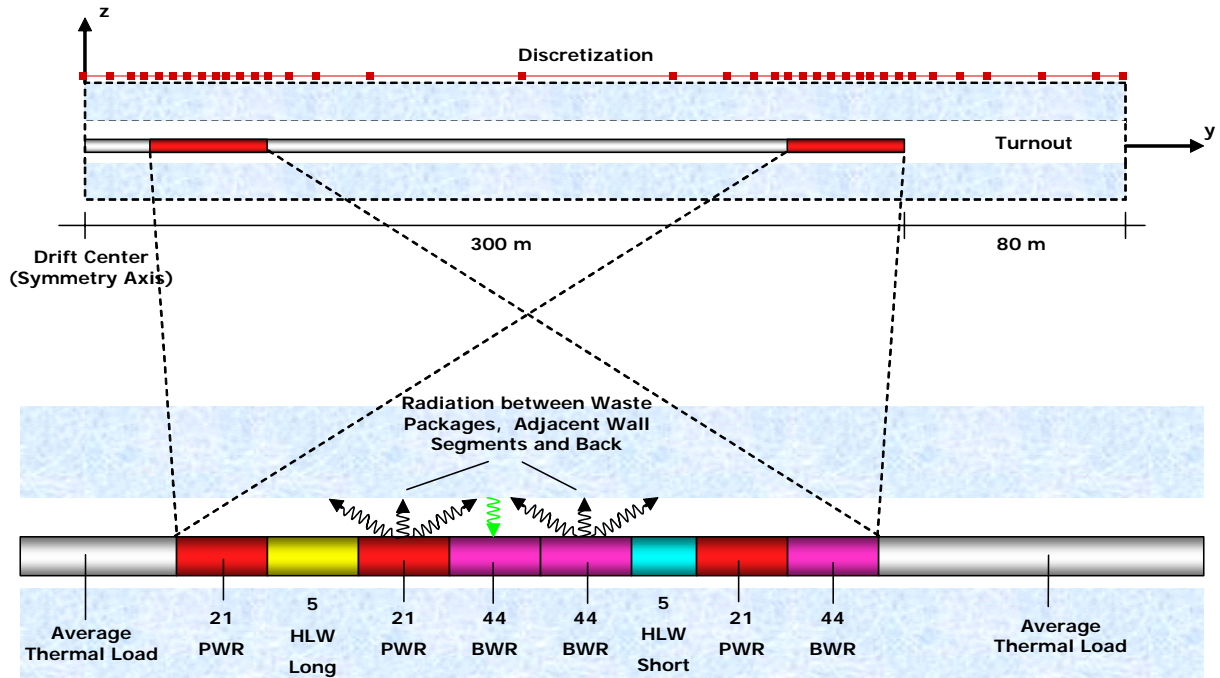
Figure 3. Schematic model geometry along emplacement drift. Red dots indicate location of vertical slices. Two segments are finely discretized to accompany individual waste packages. Notice the yellow and cyan "HLW" waste packages, which have the smallest heat output.
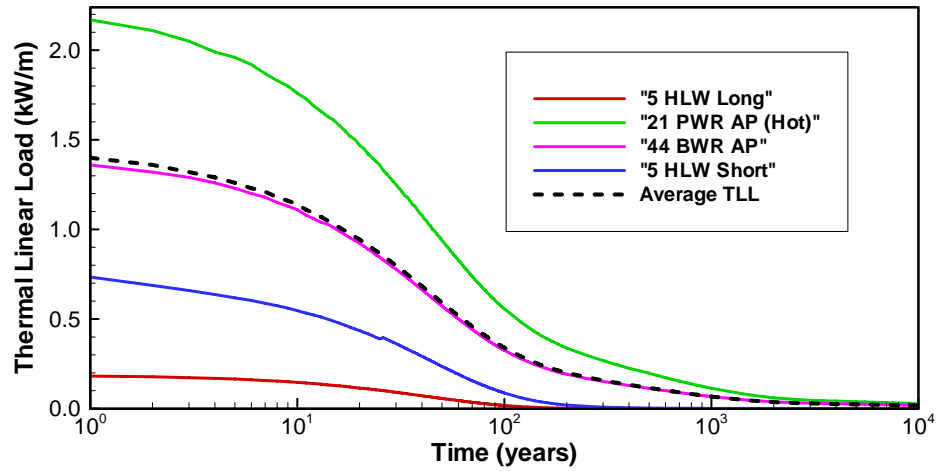
Figure 4.   Thermal load of individual waste packages as a function of time. Time zero represents the time of waste emplacement. "Average TLL" denotes average thermal line load.
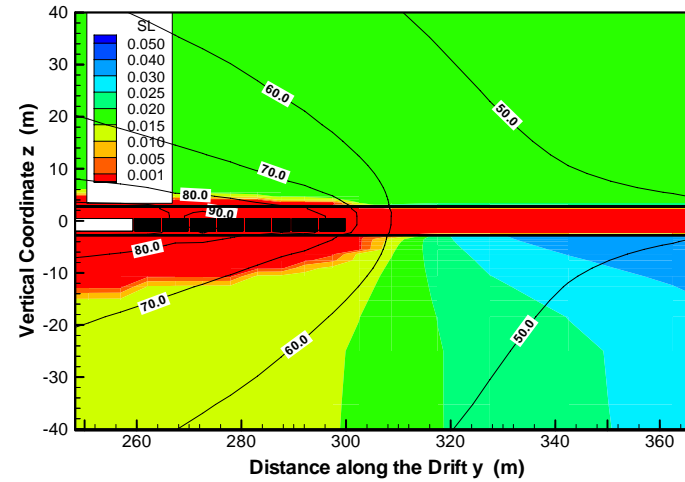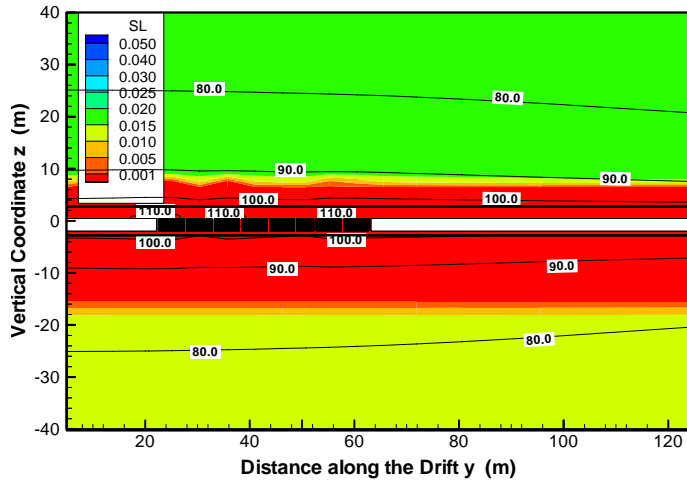
(a) Colored contours show fracture saturation; contour lines show temperature in the rock mass and in the drift.
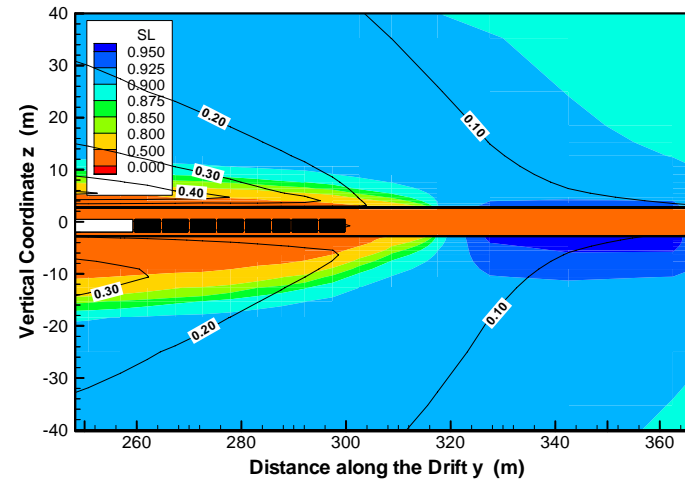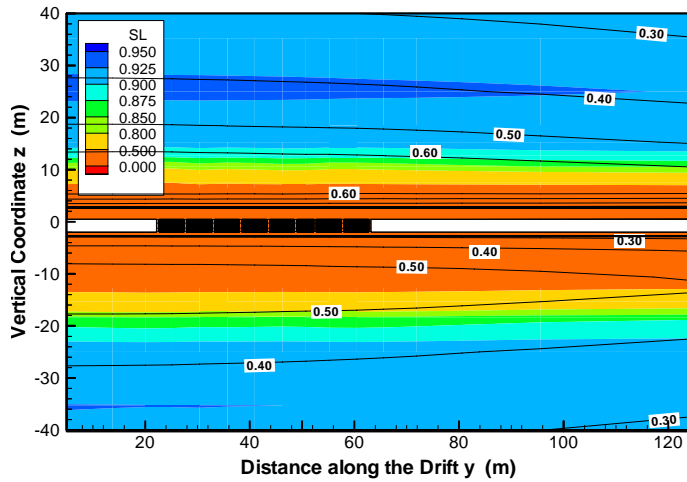
(b) Colored contours show matrix saturation; contour lines show vapor mass fraction in the matrix and in the drift.

Figure 5.   Simulated TH conditions for Case 1 (strong convective mixing) in vertical cross section along the drift after 500 years. The distance along the drift is measured with y = 0 in the center of the heated section of the drift, the symmetry boundary of the half-drift model. The heated section of the drift ends at y = 300 m, followed by an 80 m long unheated end section. Waste packages with individual heat load are shown in black. Waste packages with uniform line load are shown in white.
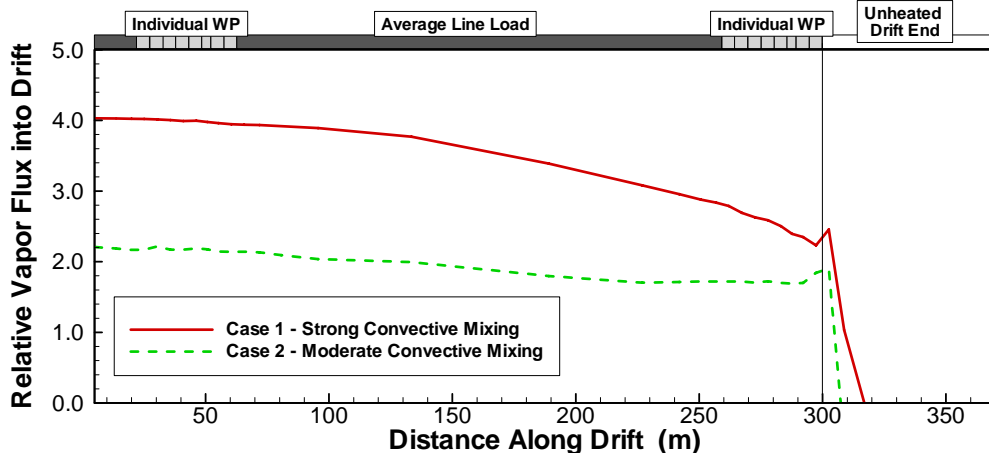
Figure 6.   Vapor flux from formation to drift at 500 years for Case 1 (solid line) and (b) Case 2 (dashed line). Vapor flux is normalized by dividing with ambient percolation flux integrated over the cross-sectional area of the drift.
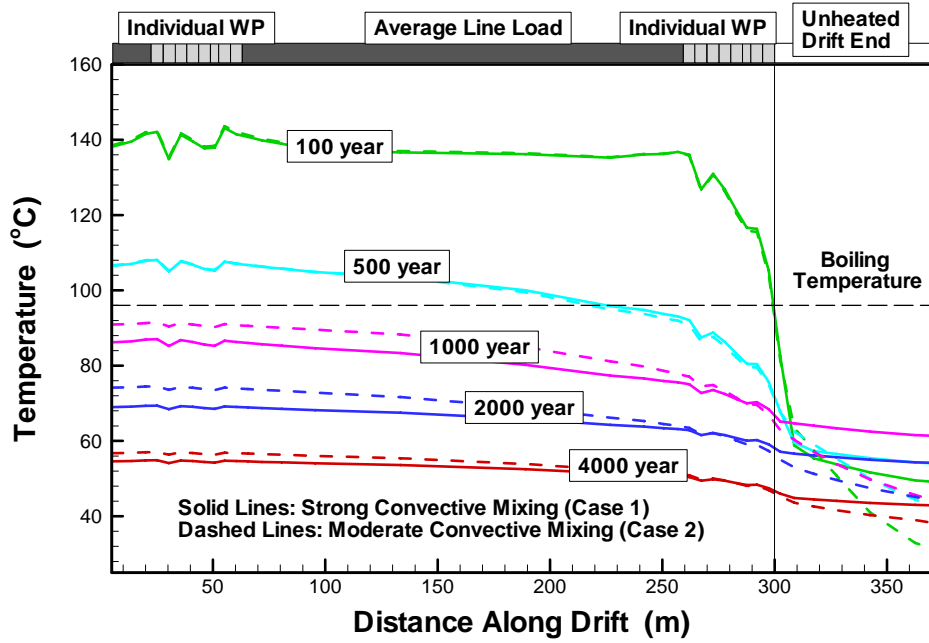
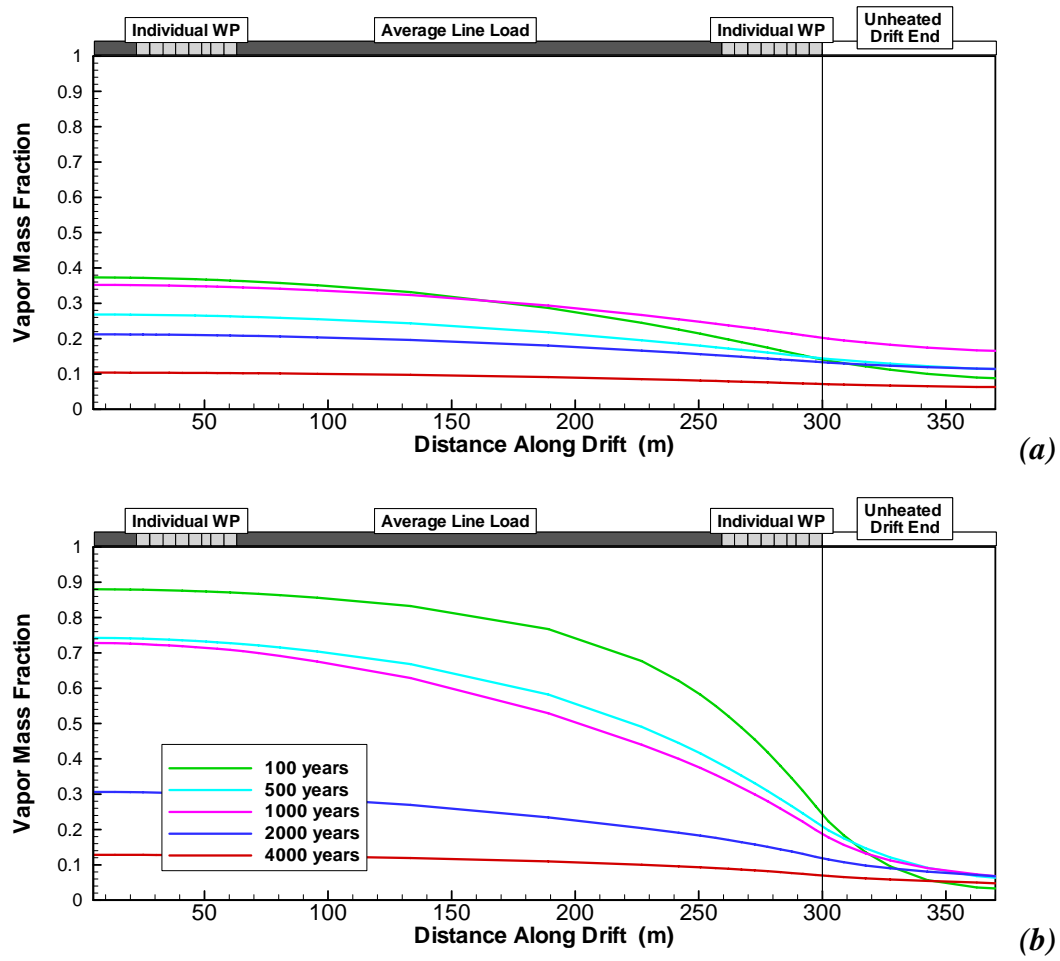*Figure 7.   Temperature along drift crown for Case 1 (solid lines) and Case 2 (dashed lines)*

Figure 8.   Vapor mass fraction along drift crown for (a) Case 1, with strong convective mixing, and (b) Case 2, with moderate convective mixing
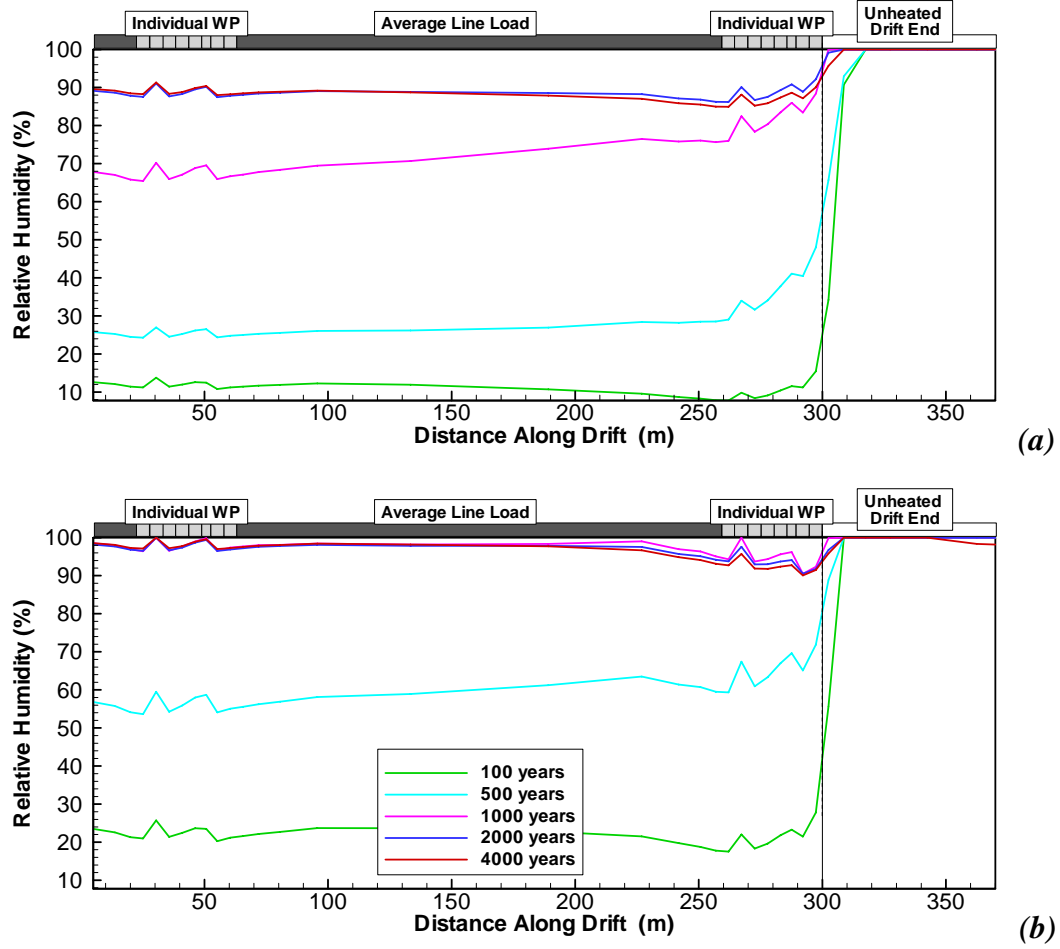
Figure 9. Relative humidity along drift crown for (a) Case 1, with strong convective mixing, and (b) Case 2, with moderate convective mixing
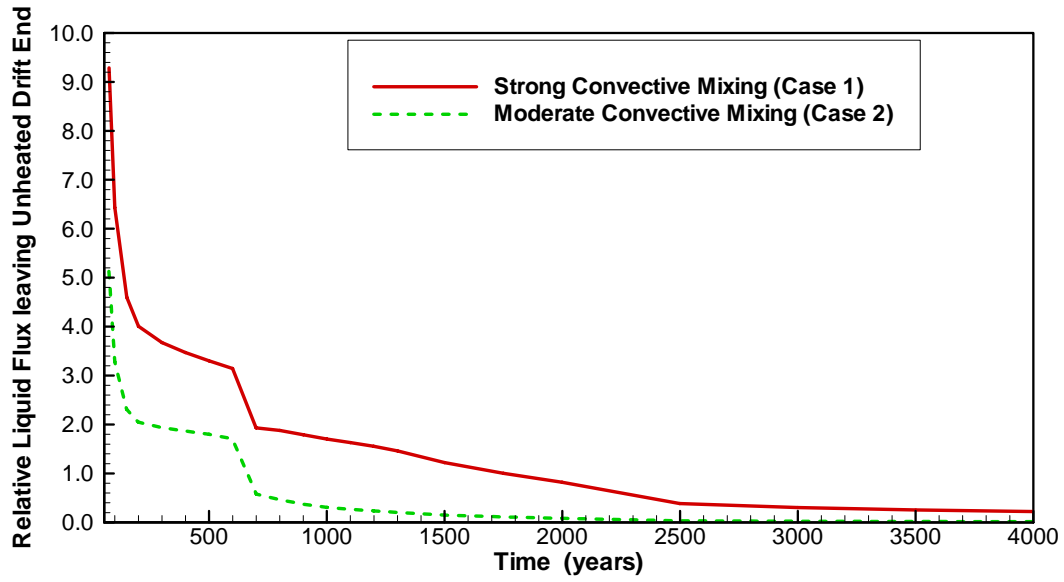
Figure 10.   Relative liquid flux leaving unheated end section of the drift for Case 1 (solid line) and (b) Case 2 (dashed line). Liquid flux is normalized by dividing with ambient percolation flux integrated over the cross-sectional area of the drift.
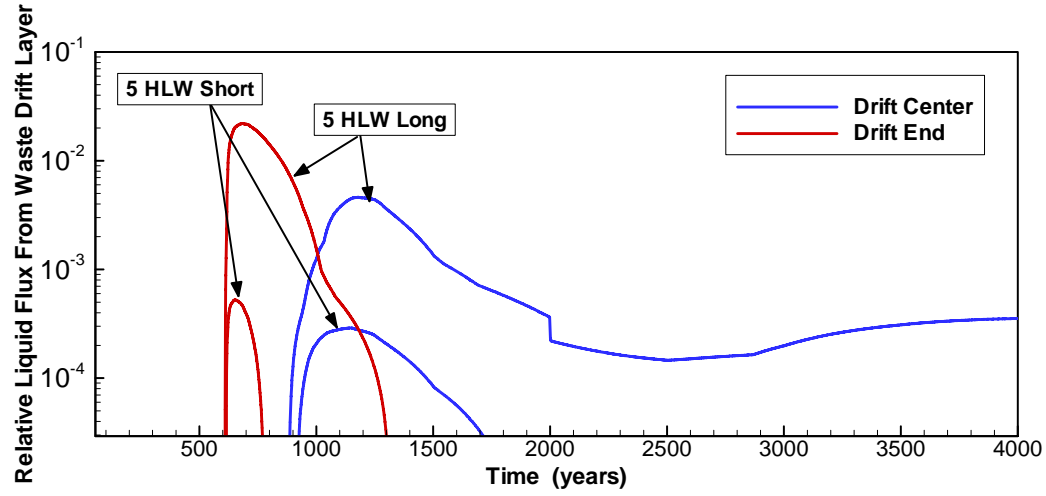
Figure 11. Evolution of relative liquid flux from waste package segments for Case 2, with moderate convective mixing. Liquid flux is normalized by dividing with ambient percolation flux integrated over the cross-sectional area of the drift.
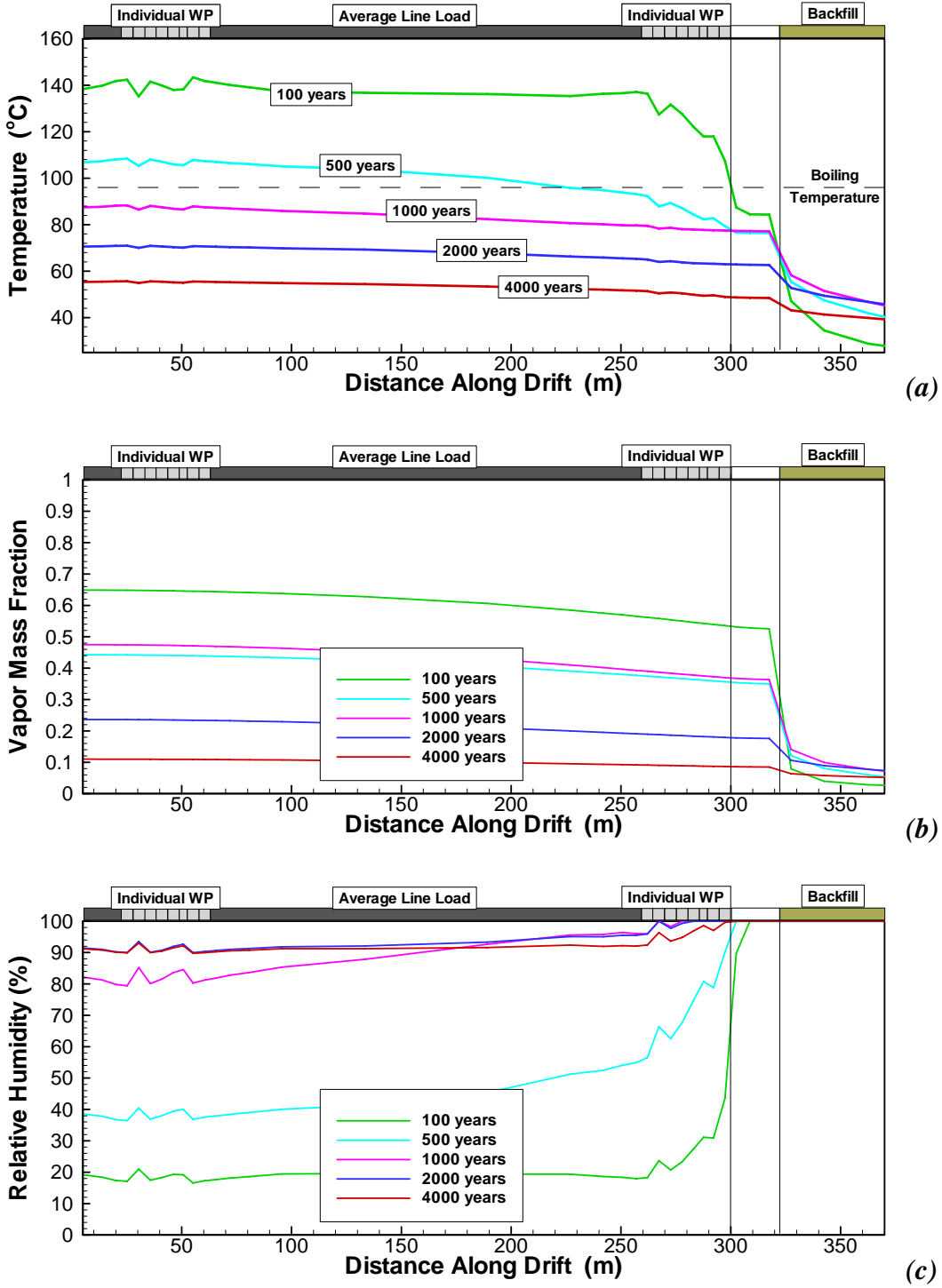
Figure 12. *Results for sensitivity case with a 20 m long end section and strong convective mixing: (a) temperature, (b) vapor mass fraction, and (c) relative humidity. As in previous cases, the heated section of the drift ends at y = 300 m, but the 80 m long drift turnout has a 20 m long open section and a 60 m long backfilled section.*
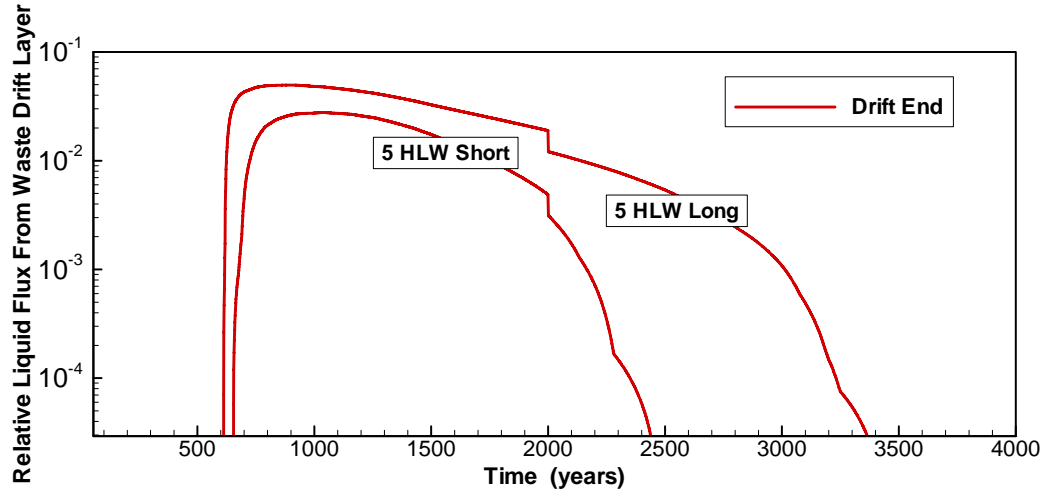
Figure 13. *Evolution of relative liquid flux from waste package segments for sensitivity case with a 20 m long end section and strong convective mixing. Liquid flux is normalized by dividing with ambient percolation flux integrated over the cross-sectional area of the drift. Local condensation occurs in the end section, not in the center section of the heated drift.*

Table 1. Mass dispersion coefficients (m^2/s) based on Webb and Itamura (2004)

Cases/Time Period (years)	300 - 600	600 – 2,000	2,000 – 4,000
Case 1: Strong convective mixing	0.1	0.1	0.1
Case 2: Moderate convective mixing	0.008	0.004	0.004